


RESOURCE

Chromoplast differentiation in bell pepper (*Capsicum annuum*) fruits

Anja Rödiger^{1,2}, Birgit Agne^{1,2}, Dirk Dobritzsch¹, Stefan Helm¹, Fränze Müller^{1,3}, Nina Pöttsch¹ and Sacha Baginsky^{1,2,*} ¹Plant Biochemistry, Institute of Biochemistry and Biotechnology, Martin-Luther-Universität Halle-Wittenberg, Halle (Saale), Germany,²Biochemistry of Plants, Biology and Biotechnology, Ruhr-University Bochum, Bochum, Germany, and³Biochemistry and Functional Proteomics, Institute of Biology II, University of Freiburg, Freiburg, Germany

Received 15 September 2020; revised 20 November 2020; accepted 24 November 2020; published online 30 November 2020.

*For correspondence (e-mail sachabaginsky@rub.de).

SUMMARY

We report here a detailed analysis of the proteome adjustments that accompany chromoplast differentiation from chloroplasts during bell pepper (*Capsicum annuum*) fruit ripening. While the two photosystems are disassembled and their constituents degraded, the cytochrome b_6/f complex, the ATPase complex, and Calvin cycle enzymes are maintained at high levels up to fully mature chromoplasts. This is also true for ferredoxin (Fd) and Fd-dependent NADP reductase, suggesting that ferredoxin retains a central role in the chromoplasts' redox metabolism. There is a significant increase in the amount of enzymes of the typical metabolism of heterotrophic plastids, such as the oxidative pentose phosphate pathway (OPPP) and amino acid and fatty acid biosynthesis. Enzymes of chlorophyll catabolism and carotenoid biosynthesis increase in abundance, supporting the pigment reorganization that goes together with chromoplast differentiation. The majority of plastid encoded proteins decline but constituents of the plastid ribosome and AccD increase in abundance. Furthermore, the amount of plastid terminal oxidase (PTOX) remains unchanged despite a significant increase in phytoene desaturase (PDS) levels, suggesting that the electrons from phytoene desaturation are consumed by another oxidase. This may be a particularity of non-climacteric fruits such as bell pepper that lack a respiratory burst at the onset of fruit ripening.

Keywords: *Capsicum annuum*, chromoplast, quantitative proteomics, plastid differentiation, chromorespiration.

INTRODUCTION

Plastids are semi-autonomous organelles that develop and differentiate from undifferentiated proplastids into different plastid types that are distinguished by their pigment content and energy metabolism, for example as photosynthetic and autotrophic or as non-photosynthetic and heterotrophic. Because of their relevance for fruit ripening and endosperm development, amyloplasts and chromoplasts received most consideration among the non-photosynthetic plastid types lately (Camara *et al.*, 1995; Waters and Pyke, 2005; Sadali *et al.*, 2019). Chromoplasts synthesize large amounts of presumably health-promoting carotenoids; therefore, research on chromoplast differentiation is dedicated to advance carotenoid biosynthesis in crops at a quantitative scale to improve their dietary quality (Taylor and Ramsay 2005; Rodriguez-

Concepcion *et al.*, 2018). Chromoplast differentiation can be reversible, such as in pumpkin (*Cucurbita pepo*) and citrus (Rutaceae) fruits, or irreversible, such as in bell pepper (*Capsicum annuum*) and tomato (*Solanum lycopersicum*). Irreversible chromoplast differentiation in the latter two species originates from fully functional chloroplasts and proceeds to mature chromoplasts by degradation of thylakoid membranes and their replacement with storage structures for carotenoids (Camara *et al.*, 1995; Egea *et al.*, 2010).

The transition from photosynthetic chloroplasts to fully differentiated heterotrophic chromoplasts requires the remodeling of an autotrophic metabolism to a heterotrophic metabolism and as such represents an integral part of the metabolic reorganizations that occur during fruit ripening (Li and Yuan 2013; Pesaresi *et al.*, 2014). Details of

this reorganization at the protein/enzyme level were initially mapped by quantitative proteome analyses in tomato, a climacteric fruit that undergoes a steep rise in respiration and ethylene production at the onset of ripening (Barsan *et al.*, 2012; Szymanski *et al.*, 2017; Quinet *et al.*, 2019). Using three stages during chromoplast differentiation, a decrease in the amount of thylakoid membrane components and carbohydrate metabolic enzymes and a rise in the abundance of stress-response proteins and carotenoid biosynthetic enzymes was reported for the chloroplast to chromoplast transition (Barsan *et al.*, 2010; Barsan *et al.*, 2012; Suzuki *et al.*, 2015). Overall, major portions of the chromoplast proteome match the occurrence of major metabolic modules in other heterotrophic plastid types such as etioplasts and amyloplasts (e.g., Neuhaus and Emes, 2000, Kleffmann *et al.*, 2007; Renato *et al.*, 2015; Ma *et al.*, 2018).

A distinctive feature of chromoplasts compared to other heterotrophic plastid types is the massive synthesis and storage of carotenoids. Recently a DnaJ-like chaperone termed ORANGE (OR) was reported to promote carotenoid biosynthesis by increasing the amount of carotenoid biosynthetic enzymes through functional interactions with the stromal Clp protease complex (Rodriguez-Concepcion *et al.*, 2019). OR promotes the correct folding of phytoene synthase (PSY) and as such increases its activity and prevents misfolding and removal by the Clp protease complex, which is similar to the anticipated function of ClpB3 in the stabilization of deoxyxylulose 5-phosphate synthase (DXS) (D'Andrea and Rodriguez-Concepcion, 2019). Furthermore, OR promotes the formation of carotenoid-sequestering structures, and also prevents carotenoid degradation. Intriguingly, OR is also nuclear-localized, where it interacts with the transcription factor TCP14 to repress chloroplast biogenesis during de-etiolation, suggesting that OR may in general be relevant for plastid-type transitions (Sun *et al.*, 2019). A post-transcriptional mechanism that could be important for chromoplast differentiation was recently suggested to comprise the remodeling of the protein import machinery by the E3 ligase Sp1 (Ling *et al.*, 2012). In this model, the ubiquitin proteasome system (UPS) disassembles the Toc159-containing translocon at the outer chloroplast membrane (TOC) complexes that sustain the import of photosynthetic proteins in chloroplasts to TOC complexes with different specificities to promote the import of chromoplast specific proteins (Sadali *et al.*, 2019).

We report here a comprehensive proteome analysis of the chromoplast differentiation process in the non-climacteric fruit bell pepper. We performed native PAGE to separate protein complexes from seven different stages during chromoplast differentiation and performed in solution analyses with the same fractions. Using protein quantification by the MS^E-based Hi3 method (Silva *et al.*, 2006; Helm

et al., 2014), we quantified proteins in every fraction in three biological replicates. Our study provides a detailed quantitative map of chromoplast differentiation at the protein level and is available as a high-resolution resource for plant biologists.

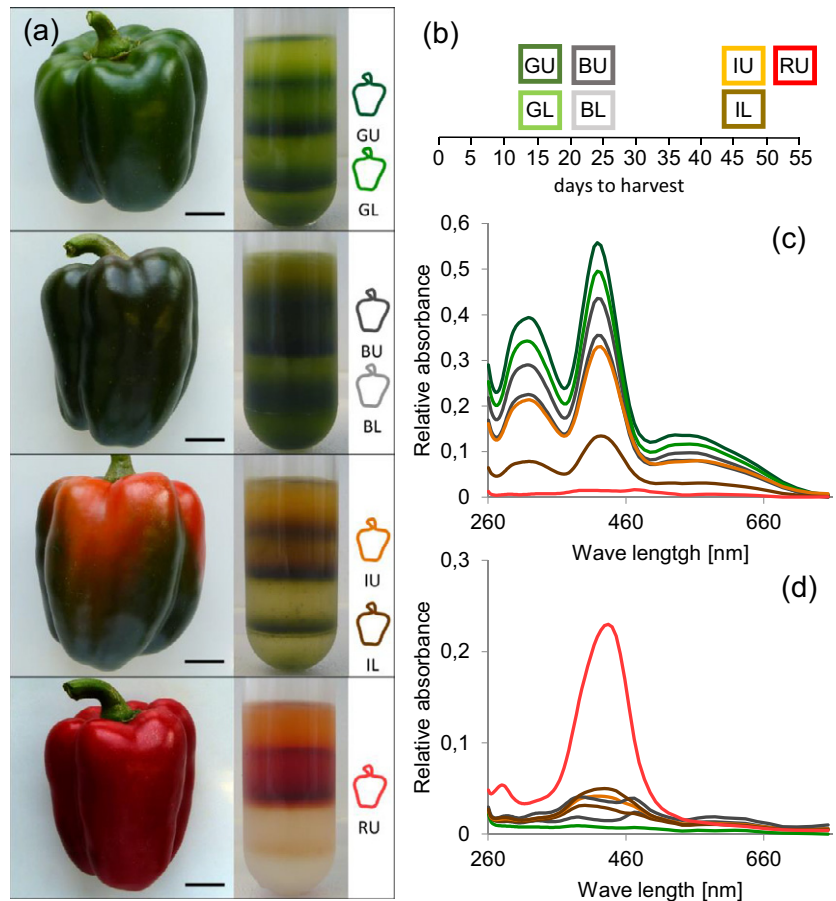
RESULTS AND DISCUSSION

Isolation of plastids from bell pepper fruits

Selma Bell, the bell pepper variety used in this study, produces full-sized green fruits within approximately two weeks after flowering, representing the initial stage of fruit ripening. About one week later, the fruit color changes into dark-green, almost black. Three to four weeks later, the fruits reach the second intermediate stage with mixed red and green colors. Within one week after this point, the fruits turn homogeneously red and are fully matured, representing the final stage of fruit development (Figure 1(a,b)). These stages were used for the isolation of plastids from ripening fruit tissue by an isolation procedure that is based on Percoll density gradient centrifugation (Siddique *et al.*, 2006). The employed step-gradient allowed the separation of plastid populations that differ by their density, distributing into an upper and a lower band (Figure 1). All plastid-containing bands were collected and named by their occurrence in the gradient as, for example, GU for green-upper band and IL for intermediate-lower band, and their pigment content was determined by HPLC combined with UV/VIS spectra measurements that were acquired in the range of 260–760 nm. Using a monitoring wavelength of 430 nm, 15 peaks were numbered in order of their occurrence, as shown in Figure S1. LC-APCI-MS was used to determine *m/z* values of these peaks. Using the combination of UV/VIS and *m/z*, 11 peaks could be identified (Figure S1, Table S1).

The differentiation of chromoplasts from chloroplasts is accompanied by the degradation of chlorophyll and the synthesis of carotenoids. We therefore assessed the pigment content of the different plastid preparations by exploring chlorophyll b (Figure 1(c) peak 5 in Figure S1) and capsanthin dimyristate (Figure 1(d) peak 7 in Figure S1) abundance. A progressive decline in chlorophyll b levels among the different preparations supported the intermediate nature of the black and red/green fruits. Together with the increase in carotenoid levels, the pigment measurements provided the following order to the different plastid preparations on their way to chromoplasts: starting from fully developed chloroplasts in GU/GL, BU, BL, IU, IL, to RU as the final stage of chromoplast differentiation. The kinetics of the capsanthin dimyristate peak shows that the most fundamental changes in carotenoid content occur relatively late, that is, between IU/IL and RU. This suggests that carotenoid biosynthesis and sequestration have their maximum during the final days of fruit ripening.

Figure 1. Bell pepper fruit ripening. (a) Bell pepper fruits harvested at different time points during fruit ripening are presented along with the corresponding Percoll gradients obtained after density gradient centrifugation of their homogenates. (b) Time-scale in days (0 representing flowering time) for the harvest, illustrated by pepper icons for the different developmental stages. All stages of maturation are represented: GL, GU, BL, BU, IL, IU, and RU. (b, c) Kinetics of changes in pigment content are illustrated for the chloroplast specific chlorophyll b peak (c) and the chromoplast specific peak of the carotenoid diester capsanthin dimyristate (d). Abbreviations: G, green; B, black; I, intermediate; R, red; L, lower; U, upper.



Consistently, we identified several compounds characteristic for fully ripe red fruits, for example, capsanthin/capsorubin-laurate, zeaxanthin dipalmitate, and zeaxanthin laurate myristate, exclusively at the last maturation stage (Figure S1, Table S1, peaks 11–13). In contrast, there was a slow decline in chlorophyll content, suggesting that chlorophyll degradation occurs throughout the entire chloroplast differentiation process.

Protein complex reorganization during progressive chloroplast differentiation

We extracted proteins from the seven different plastid preparations and subjected the protein fractions to colorless native (CN)-PAGE. The distribution of protein complexes supports progressive chloroplast differentiation in the order inferred by the pigment measurements (see above, Figures 1 and 2). To determine the identity of the visualized protein complexes, we identified and quantified proteins from the GL and the RU lanes from 16 gel pieces by MS^E analysis (Silva *et al.*, 2006; Helm *et al.*, 2014) (Figure 2, Figure S2). The abundant complexes visible in the GL lane comprise photosystem II (PSII) and PSI subunits that decrease in abundance from GL/GU to BL, BU, IL, and

IU. In the RU stage, these complexes are no longer visible (Figure 2). Prominent low-molecular mass protein bands that appear approximately at the IL stage dominate this preparation.

For the purpose of a rapid automated functional annotation by MapMan (Thimm *et al.*, 2004), we matched the identifications to the *Arabidopsis thaliana* database TAIR10. The identity of individual proteins in the different gel fractions is provided in Table S2. Initial screening of the quantitative data suggested that the cytochrome *b₆f* complex, ATPase, and other electron carriers (bin 1.1.5) are sustained from chloroplasts to fully developed chromoplasts (Table S2, Figure S2). Enzymes involved in carotenoid biosynthesis are significantly upregulated, together with plastoglobule-associated proteins for carotenoid sequestration. Reproducibility of protein quantification in proteomics approaches suffers from large numbers of experimental interventions. We therefore decided to move ahead with our analysis by performing a single-step in solution digestion with the seven plastid preparations detailed above, and inferring proteome adaptations during chloroplast differentiation from these data (see below).

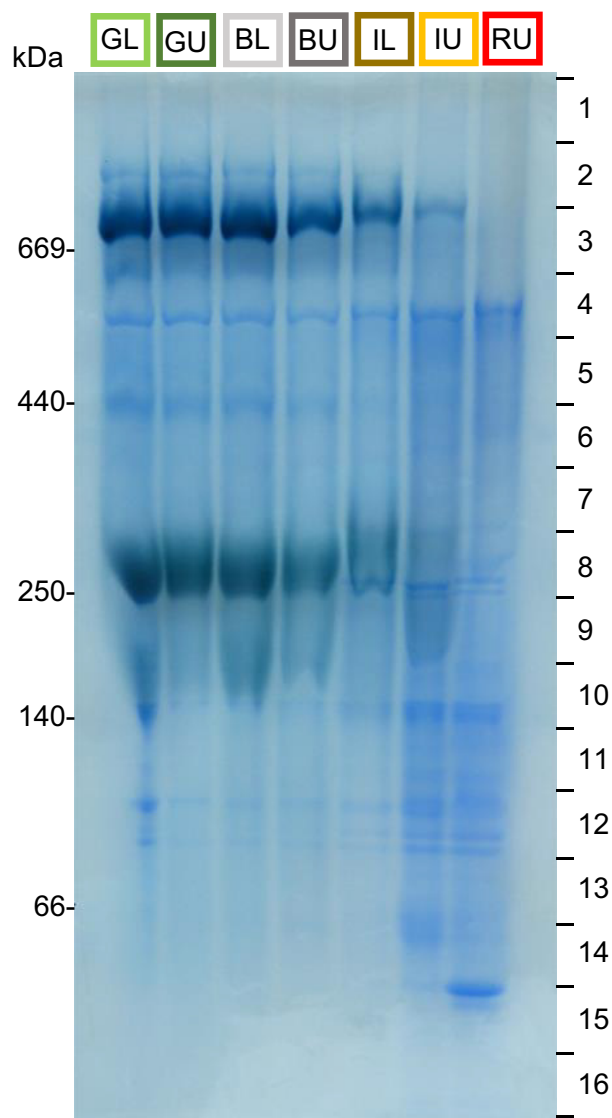


Figure 2. Native protein complexes during chromoplast differentiation. Colorless native PAGE of extracts from isolated plastids obtained from the different developmental stages as detailed in Figure 1(b). The gel was stained with Coomassie and subsequently cut into 16 pieces for tryptic digestion and mass spectrometric protein identification, as indicated.

Proteome abundance dynamics during progressive chromoplast differentiation

Protein extracts from the plastid samples obtained at different ripening stages were compared by their protein patterns on SDS-PAGE (Figure 3(a)). While the chloroplast samples are dominated by low-molecular mass light-harvesting complex proteins, the chromoplast samples accumulate increasing amounts of capsanthin/capsorubin synthase (CCS) at approximately 50 kDa (Siddique *et al.*, 2006). This enzyme is the most abundant protein in chromoplasts, supporting the highly active carotenoid

biosynthesis in this plastid type (A0A089N971, Table S3). The decrease of the LHC band at 25–30 kDa and the increase of the CCS band at 50 kDa supports a progressive transition between the plastid types represented by our samples (Figure 3(a)). We used these fractions for an in solution digestion and performed quantitative proteomics by matching the MS data against the UniProt bell pepper proteome database (UP000222542) using an internal abundance marker for Hi3-based absolute protein quantification (see also above, Silva *et al.*, 2006; Helm *et al.*, 2014). Altogether we performed three biological replicates with three technical replicates each, giving rise to a cumulative identification of 2537 proteins after removal of spurious detections (<1 fmol sum in all fractions), histone proteins, and cytosolic ribosome contaminations.

We performed Target P 2.0-based localization prediction with the identified proteins for a rough assessment of every preparation's purity. In contrast to recent bell pepper proteome analyses that matched bell pepper sequences back onto Arabidopsis and performed targeting prediction with the Arabidopsis sequences (e.g., Wang *et al.*, 2013) we performed the prediction on UniProt-deposited bell pepper sequences. In total, we identified 1010 unique plastid predicted and plastid encoded proteins (Table S3). All preparations derived from the *lower bands* in the density gradients contain between 62% and 66% predicted plastid proteins that distribute to around 75% of total protein mass in these fractions (Figure S3). Only 2–3% of the proteins are predicted to localize to mitochondria and/or the secretory pathway (Table S3, Figure S3), while 27–30% are predicted for 'other' localizations. These proteins comprise cytosolic contaminants and plastid proteins with transit peptides that are not recognized by Target P 2.0 (Almagro Armenteros *et al.*, 2019). The preparations obtained from the *upper band* contain 5–7% mitochondrial, 3–5% secretory pathway, and 36–44% 'other' predicted proteins, indicating a higher extent of mitochondrial contaminations. However, the *upper band* preparations contain between 60% and 70% protein mass allocated to plastid proteins, suggesting that the contaminations are of minor abundance (Figure S3).

We used the quantitative proteome data to assess the similarity between the different plastid types by hierarchical clustering using a Pearson correlation distance metric (Figure 3(b)). To avoid a potential bias by the different degrees of impurity in the *upper* and *lower* fractions, we exclusively clustered plastid proteins (plastid encoded and plastid predicted, Table S3). The plastid types cluster into two main clusters, one comprising the stages GL, GU, BL, BU, and IL and the second comprising the IU and RU stages. Within each of the two clusters, the plastid types are very similar with Pearson correlation coefficients > 0.8 (Figure 3(b)). Surprisingly, the two intermediate stages IL and IU are clearly distinct despite having the same age

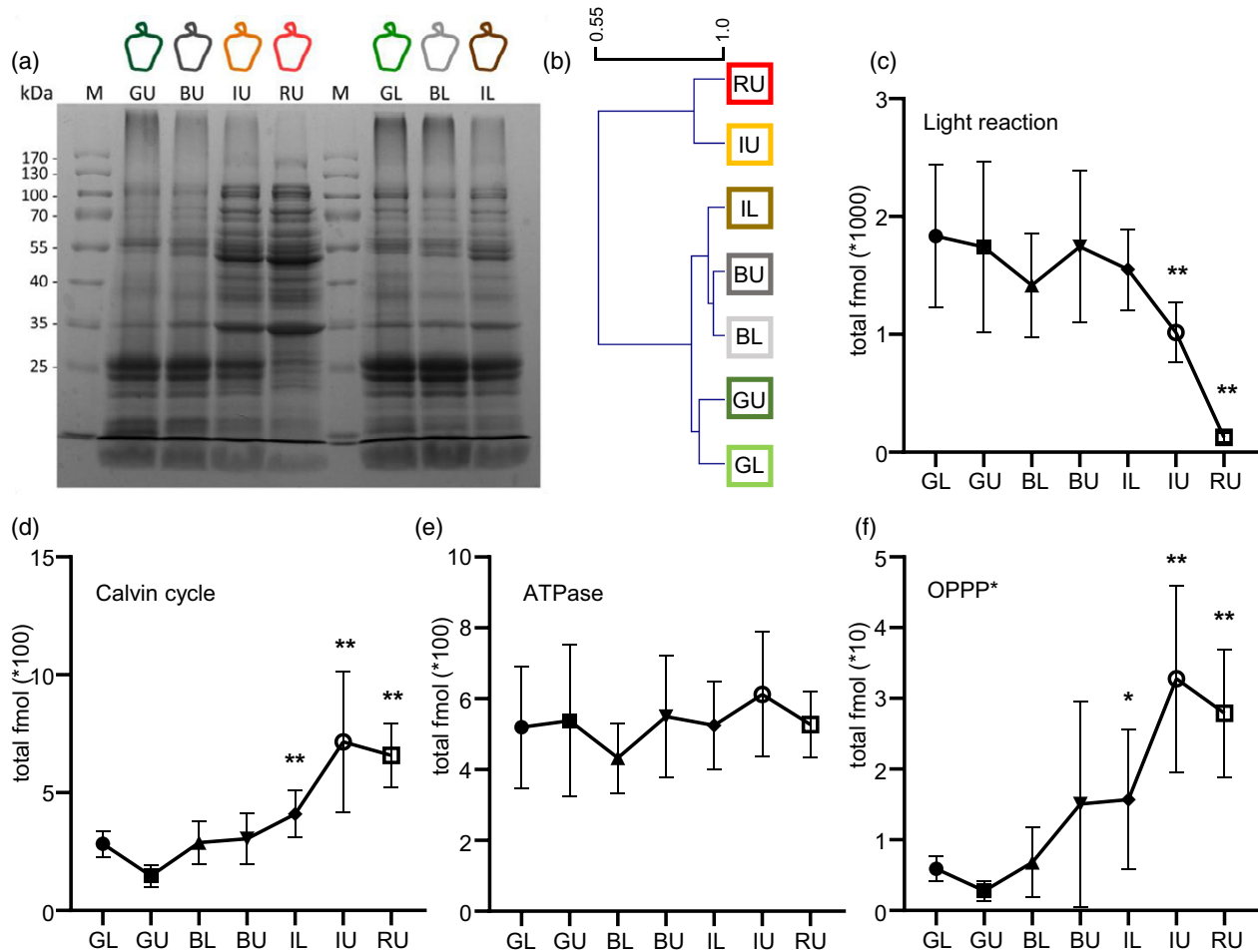


Figure 3. Protein profiles and protein abundances in plastids from different ripening stages. (a) SDS-PAGE displaying protein profiles obtained from the different developmental stages during fruit ripening (see Figure 1(b)). (b) Results of a hierarchical cluster of the different plastid types ('sample' clustering) with Pearson correlation as distance metric. (c–f) Total abundance of proteins involved in the different pathways/functional categories of primary energy metabolism in the different plastid preparation, i.e., light reactions of photosynthesis encompassing photosystems I and II and LHC proteins (c), Calvin cycle enzymes (d), ATPase subunits (e), and the oxidative branch of the pentose phosphate pathway (f) (*glucose-6-phosphate 1-dehydrogenase [A0A1U8HAS8, A0A1U8GPM1] and 6-phosphogluconate dehydrogenase [A0A2G2Y8Q9, A0A2G2Y8R9, and A0A1U8F1N4]). Significant differences with the GL sample (as chloroplast reference) are highlighted by one (P -value < 0.05, t -test [Welch test], two-sided) or two stars (P -value < 0.005, t -test [Welch test], two-sided) on top of the columns. Error bars represent SD.

(47 days, see Figure 1(b) for reference), suggesting that the intermediate stage of fruit ripening comprises two different plastid types within one fruit. This is similar to the situation found in tomato, where the intermediate, yellow ripening stage contained chloroplasts and chromoplasts at the same time (Camara *et al.*, 1995). In contrast to tomato, the two plastid types are not interspersed in pepper but rather confined to different sections in the fruit.

The most significant adaptation of the chloroplast proteome to a heterotrophic chromoplast metabolism is the disassembly of the photosynthetic machinery, as shown in Figure 2 and in Figure 3(c). Notably, the protein constituents of the light reactions of photosynthesis are

maintained up to the IL stage before they decline rapidly in the IU and RU stages (Figure 3(c)). In contrast, constituents of the Calvin cycle and ATPase are maintained at high abundance throughout the entire differentiation process. In the case of ATPase this suggests that fully mature chromoplasts synthesize ATP at a high rate (see also the discussion below, Figure 3(d,e)). Similar to other heterotrophic plastid types, the oxidative branch of the oxidative pentose phosphate pathway (OPPP) is significantly elevated in chromoplasts (Figure 3(f)), supporting the previous notion that a substantial amount of reducing power in heterotrophic plastids is generated by NADP reduction through OPPP activity (Neuhaus and Emes, 2000; von Zychlinski

et al., 2005). An active pentose phosphate metabolism is further supported by elevated transaldolase and transketolase abundance in chromoplasts, the latter being one of the most abundant chromoplast enzymes (Siddique *et al.*, 2006, Table S3, here depicted within the Calvin cycle (Figure 3(d)).

High OPPP activity in chromoplasts can be also inferred from the central role of ferredoxin (Fd) in the bell pepper chromoplast redox metabolism (Figure 4). The abundance of ferredoxin, Fd-dependent NADPH reductase (FNR), and Fd-dependent glutamate synthase increases in the course of chromoplast differentiation (Figure 4), which is counter-intuitive because ferredoxin reduction relies on photosynthetic electrons that are not available at high supply in chromoplasts. It was demonstrated that root-type FNRs are able to reduce ferredoxin with electrons from NADPH (Green *et al.*, 1991), suggesting that ferredoxin reduction in chromoplasts occurs with electrons from NADPH through the activity of a root-type FNR. Indeed, one out of two identified chromoplast FNRs (AOA1U8FJG3) has 79% identity to Arabidopsis root-type FNR1 (AT4G05390). Thus, NADPH generated through OPPP activity reduces ferredoxin, thereby feeding electrons into amino acid biosynthesis through Fd-dependent glutamate synthase (Figure 4). Amino acid biosynthesis is a dominant metabolic activity in chromoplasts (Table S3) as well as in other heterotrophic plastid types (Neuhaus and Emes, 2000, Baginsky *et al.*, 2004; von Zychlinski *et al.*, 2005; Siddique *et al.*, 2006). Amino acid profiling at the onset of ripening reported a clear increase of 18 analyzed amino acids (Osorio *et al.*, 2012), thus documenting the requirement for high amino acid biosynthetic activities.

High carotenoid biosynthesis is a hallmark of bell pepper fruit ripening. Carotenoids are sequestered to membranes; thus, high fatty acid biosynthetic activity is necessary to sustain membrane biogenesis to accommodate storage carotenoids. The plastid encoded acetyl-CoA carboxylase subunit AccD is significantly upregulated during chromoplast differentiation (Figure 4). AccD is essential for chloroplast fatty acid metabolism since it catalyzes the first committed step of fatty acid biosynthesis, that is, carboxylation of acetyl-CoA to malonyl-CoA. This plastid encoded protein has the highest translation rate in chromoplasts of tomato (Kahlau and Bock, 2008). Our proteomics data show that AccD is only moderately more abundant in chromoplasts compared to chloroplasts, while other plastid encoded proteins, for example, components of the plastid ribosome, remain abundant in chromoplasts as well (Figure 4). The upregulation of fatty acid synthesis is paralleled by an increase of proteins involved in carotenoid biosynthesis as exemplified for phytoene synthase (PSY), phytoene desaturase (PDS), and the DnaJ-like chaperone ORANGE (OR) (Figure 4).

Plastoglobules are important for carotenoid sequestration (reviewed in van Wijk and Kessler, 2017). We found a

32-kDa fibrillin that was significantly upregulated during chromoplast differentiation, consistent with its function in plastoglobule structural organization and chromoplast pigment accumulation (Figure 4). Recently, identification of ζ -carotene desaturase, lycopene β -cyclase, and β -carotene β -hydroxylases operating in plastoglobules of chromoplasts suggested that plastoglobules function as both lipid biosynthesis and storage compartments (van Wijk and Kessler, 2017). The investment in structures for carotenoid sequestration goes together with an increasing abundance of chlorophyll-degrading enzymes, as exemplified for pheophorbide a oxygenase (PaO) (Kuai *et al.*, 2018) (Figure 4).

Chromorespiration

As in previous proteome analyses with tomato, our data show that the chloroplast ATPase is maintained at high levels, similar to the cytochrome b_6f complex (Figure 3(e) and Figure 4) (Barsan *et al.*, 2012). Several proteins involved in the thylakoid electron transport chain and ATP synthesis, e.g., cytochrome b_6f complex, plastid terminal oxidase (PTOX), and NAD(P)H dehydrogenases, were previously considered to contribute to chromoplast ATP synthesis (Pateraki *et al.*, 2013; Renato *et al.*, 2014). It is conceivable that electrons are transferred into the chromoplast membrane system at a high rate, because phytoene desaturase (PDS) catalyzes two consecutive dehydrogenation reactions with phytoene, transferring the electrons to plastoquinone (PQ) (Niegelstein *et al.*, 1995; Norris *et al.*, 1995). Thus, with the dramatic increase in PSY and PDS observed here (Figure 4), a massive transfer of electrons into the PQ pool is likely to occur during carotenoid biosynthesis. A recent model suggested that these electrons are partly scavenged by PTOX, which transfers excess electrons to O_2 , giving rise to H_2O (Josse *et al.*, 2000). This model is mostly based on the observation that PTOX is present in fully differentiated chromoplasts and its abundance increases during tomato chromoplast development. PTOX activity is responsible for one quarter of total fruit oxygen consumption in fully ripe tomato fruits (Shahbazi *et al.*, 2007; Renato *et al.*, 2014; Nawrocki *et al.*, 2015).

A similar conclusion has been reached for bell pepper since the expression of PDS, zeta-carotene desaturase, and PTOX is co-regulated at the transcriptional level (Renato *et al.*, 2015). Our data show, however, that PDS and PSY abundance on the one hand and PTOX abundance on the other hand are uncoupled at the protein level. While PDS and PSY abundances increase significantly, as does the abundance of other carotenoid biosynthetic enzymes, PTOX abundance is rather constant during chromoplast differentiation (Figure 4). Thus, it is possible that the electrons from phytoene pass through the cytochrome b_6f complex at a high rate, adding a supplementary proton pumping site and being used by plastocyanin and a

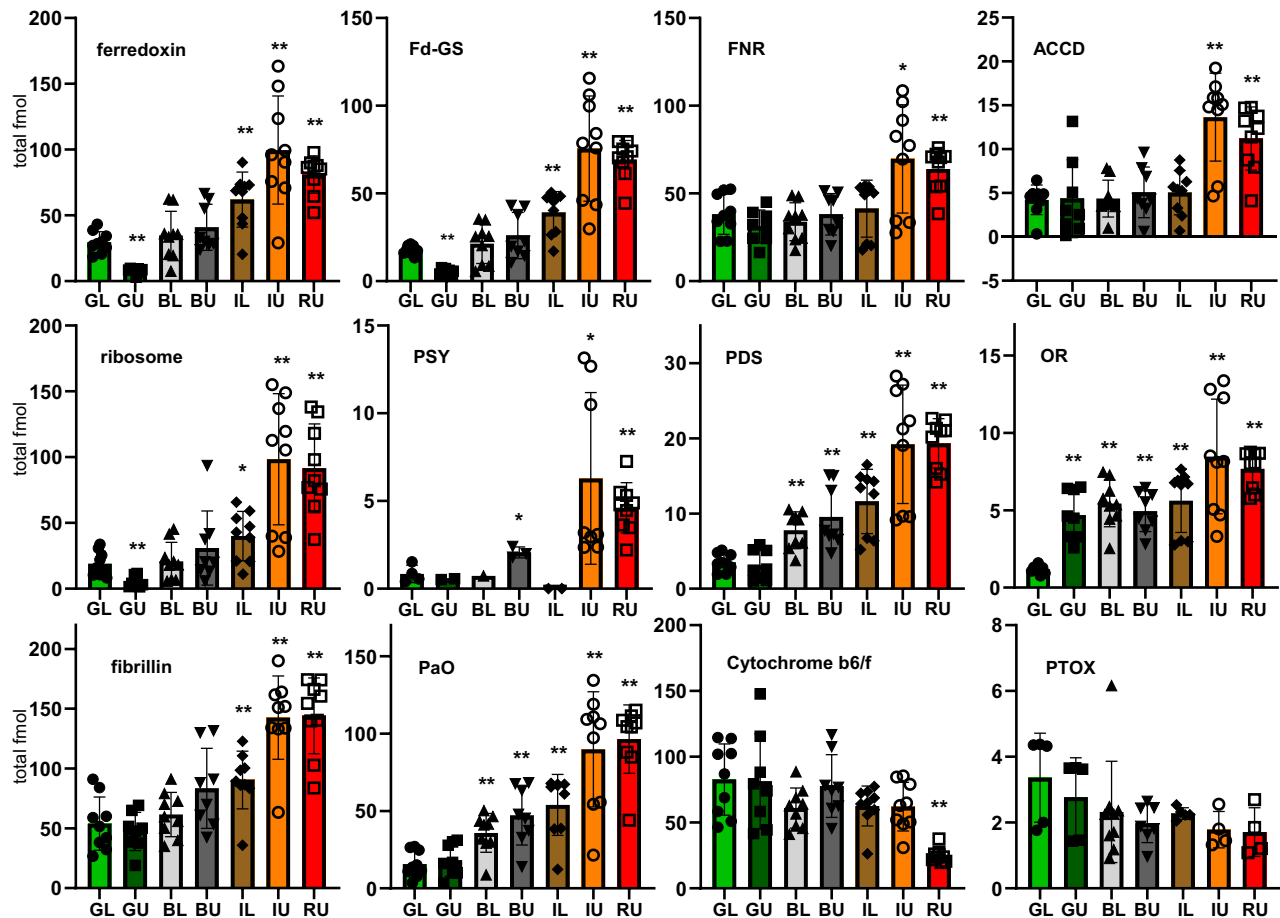


Figure 4. Abundance of selected proteins as determined from the in solution digestions with the different plastid preparations. Provided are abundances (in fmol) from three biological replicates (three technical replicates each) along with the standard deviation (SD) of the repeat measurements and the individual data points. The plastid preparations are represented by their abbreviation as in Figure 1 and additionally color-coded. The following proteins/enzymes are presented: ferredoxin (A0A1U8GXA1, A0A1U8H397, A0A2G2YH86, A0A1U8DVL9, B1PDK3, and A0A2G2XUS9), Fd-dependent glutamate synthase (Fd-GS; A0A2G3ANJ0 and A0A2G2ZX64), Fd-dependent NADP reductase (FNR; A0A1U8FJG3 and A0A1U8FMQ7), acetyl CoA-carboxylase (ACCD; A0A2G2ZQ00 and A0A2G2Z7T4), plastid 70S ribosome (ribosome; see Table S2), phytoene synthase (PSY; A0A1U8FLW3 and A0A1U8GGI5), phytoene desaturase (PDS; A0A1U8FU73), ORANGE (OR; A0A1U8FXL9 and A0A2G2ZY11), fibrillin (Q42493), pheophorbide a oxygenase (PaO; A0A2G2YHJ4), cytochrome b_6/f complex (see Table S2), and plastid terminal oxidase (PTOX; A0A2G2Y4F7). Significant differences with the GL sample (as chloroplast reference) are highlighted by one (P -value < 0.05 , t -test [Welch test], two-sided) or two stars (P -value < 0.005 , t -test [Welch test], two-sided) on top of the columns.

currently unidentified oxidase. This hypothesis is supported by the effect of a cytochrome b_6/f inhibitor on chloroplast ATP synthesis (Renato *et al.*, 2014) and by the detection of high concentrations of plastocyanin in our chloroplast preparations (Table S3). To identify other proteins that are closely co-regulated with PDS, we performed hierarchical clustering using a Pearson correlation distance metric. This clustering resulted in one cluster branch that contains a set of enzymes highly upregulated in the course of chromoplast differentiation (Figure 5). It comprises carotenoid biosynthetic enzymes, enzymes involved in fatty acid metabolism, the chaperone ClpB3, the plastid division protein FtsZ, the chlorophyll degrading enzyme PaO, and fibrillin (Figure 5). Thus, this cluster branch concisely summarizes key features of chromoplast differentiation (see above), but we did not identify a previously unknown

oxidase that may serve as the electron acceptor site for phytoene desaturation.

Organization of the protein import machinery during chloroplast to chromoplast differentiation

The plastid protein import machinery is essential for chloroplast biogenesis and recent data advocated its reorganization during plastid differentiation to accommodate the changing requirements on import specificity originating from new import cargo. The UPS is thought to be involved in this process by removing TOC components that are labeled for degradation by the E3 ubiquitin ligase Sp1, thus enabling their replacement by other TOC subunits with different precursor specificities (Sadali *et al.*, 2019). While comprehensive analyses have questioned a clear substrate specificity of individual TOC subunits

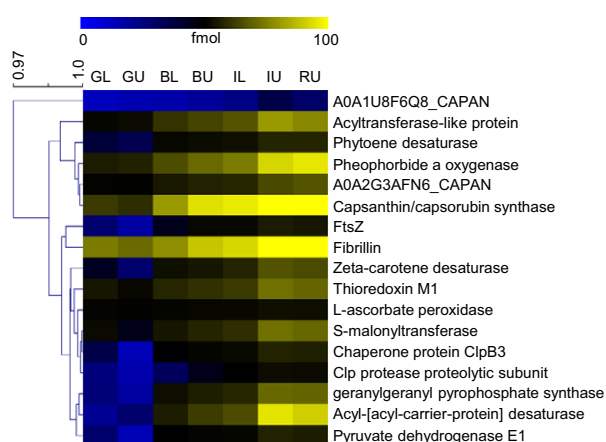


Figure 5. Hierarchical cluster around phytoene desaturase. We performed hierarchical clustering with all identified chloroplast proteins to identify co-regulated functional modules using a Pearson correlation distance metric. The presented branch of the cluster shows those proteins that are tightly co-regulated with phytoene desaturase in the course of chloroplast differentiation.

(Bischof *et al.*, 2011; Dutta *et al.*, 2014; Grimmer *et al.*, 2020), the importance of Toc159 during de-etiolation and seed germination was clearly demonstrated (Ling *et al.*, 2012; Shanmugabala *et al.*, 2018).

The bell pepper Toc159 homolog was identified at low concentrations in only one to two replicates in the GL and GU samples, thus hampering its quantification. In contrast, the Toc75 and Toc33/34 homologs were identified at all stages during chloroplast differentiation (Figure 6(a)). Their abundance is slightly higher in the IU and RU samples compared to the other plastid preparations (Figure 6), supporting conservation of the TOC machinery in chloroplasts. A better coverage of TOC subunits was achieved in the CN-PAGE analysis (Table S4). Here, Toc159, Toc75, and Toc33/34 were identified reproducibly in the high-molecular mass region of the gel (gel slices CN1–CN3, Figure 6(b), see also Schäfer *et al.*, 2019). In these complexes, the ratio between Toc159 and Toc75 was not altered between chloroplasts and chloroplasts, thus there is no indication for a reorganization of the TOC apparatus (Figure 6(b)). A comparison of transit peptides revealed no difference in the major amino acid composition of the 100 most abundant proteins in the GL and RU plastids (Figure S4); thus, major shifts in specificity may not be required for the import of chloroplast proteins. Nonetheless, we cannot exclude that TOC complexes with the bell pepper homologs of Toc132 or Toc120 may be more abundant in chloroplasts compared to chloroplasts, since we did not detect any large GTPases other than Toc159 (Agne and Kessler, 2009). In conclusion, while it is clear that Toc159 is incorporated in high-molecular mass TOC complexes in

chloroplasts (Figure 6(b)), it remains unclear whether chloroplast protein import is additionally sustained by alternative TOC complexes.

Recent data suggested that the plastid gene expression machinery keeps producing AccD (see above). Recent results suggested however that YCF1 and YCF2 are essential for plastid functioning because both are components of the protein import machinery, YCF1 as a component of a 1-MDa translocase at the inner envelope membrane and YCF2 as a component of a 2-MDa ATP hydrolysis complex associated with the translocon at the inner chloroplast membrane (TIC) complex (Kikuchi *et al.*, 2013; Kikuchi *et al.*, 2018). The protein import machinery must be maintained to support the reorganization of the plastid proteome during chloroplast development (Figure 6(a,b)). This encompasses, e.g., the massive import of carotenoid biosynthetic enzymes that are, without exception, nuclear encoded. With the exception of low amounts of plastid encoded YCF1 and YCF2, no other TIC subunits were identified (Figure 6(c)). In conclusion, chloroplast gene expression is required to sustain chloroplast metabolic functions, which is consistent with a continuous high abundance of the plastid ribosome during chloroplast differentiation as detected here (Figure 4).

Concluding remarks

The quantitative proteome analysis reported here provides a high-resolution documentation of the chloroplast differentiation process in non-climacteric bell pepper fruits. This complements earlier quantitative proteome analyses of chloroplast differentiation in the climacteric fruit tomato. A comparison between bell pepper and tomato datasets can provide insights into the molecular basis of these different ripening processes within plastids and therefore is of agronomic interest (e.g., Figure S5). Our data confirm some observations made in tomato such as changes in the levels of enzymes involved in carotenoid biosynthesis, tetrapyrrole biosynthesis, and chlorophyll degradation (Table S3, Figure S5(a)). While photosynthetic proteins progressively decline, typical enzymes of the heterotrophic plastid metabolism such as fatty acid and amino acid biosynthesis increase in abundance. In contrast to tomato, the bell pepper chloroplast redox metabolism appears to involve ferredoxin as a central redox hub. This is inferred from increasing abundance of OPPP enzymes and the continuous high abundance of ferredoxin and Fd-dependent enzymes during chloroplast differentiation (Figures 3 and 4, Table S3). During tomato fruit ripening, neither OPPP nor ferredoxin abundances were found elevated (Figure S5(b), Barsan *et al.*, 2012). Tomato chloroplasts contribute to cellular ATP synthesis and therefore represent bio-energetic organelles (Renato *et al.*, 2014). Similarly, bell pepper chloroplasts maintain high concentrations of ATPase and the cytochrome b_6/f complex, and in contrast

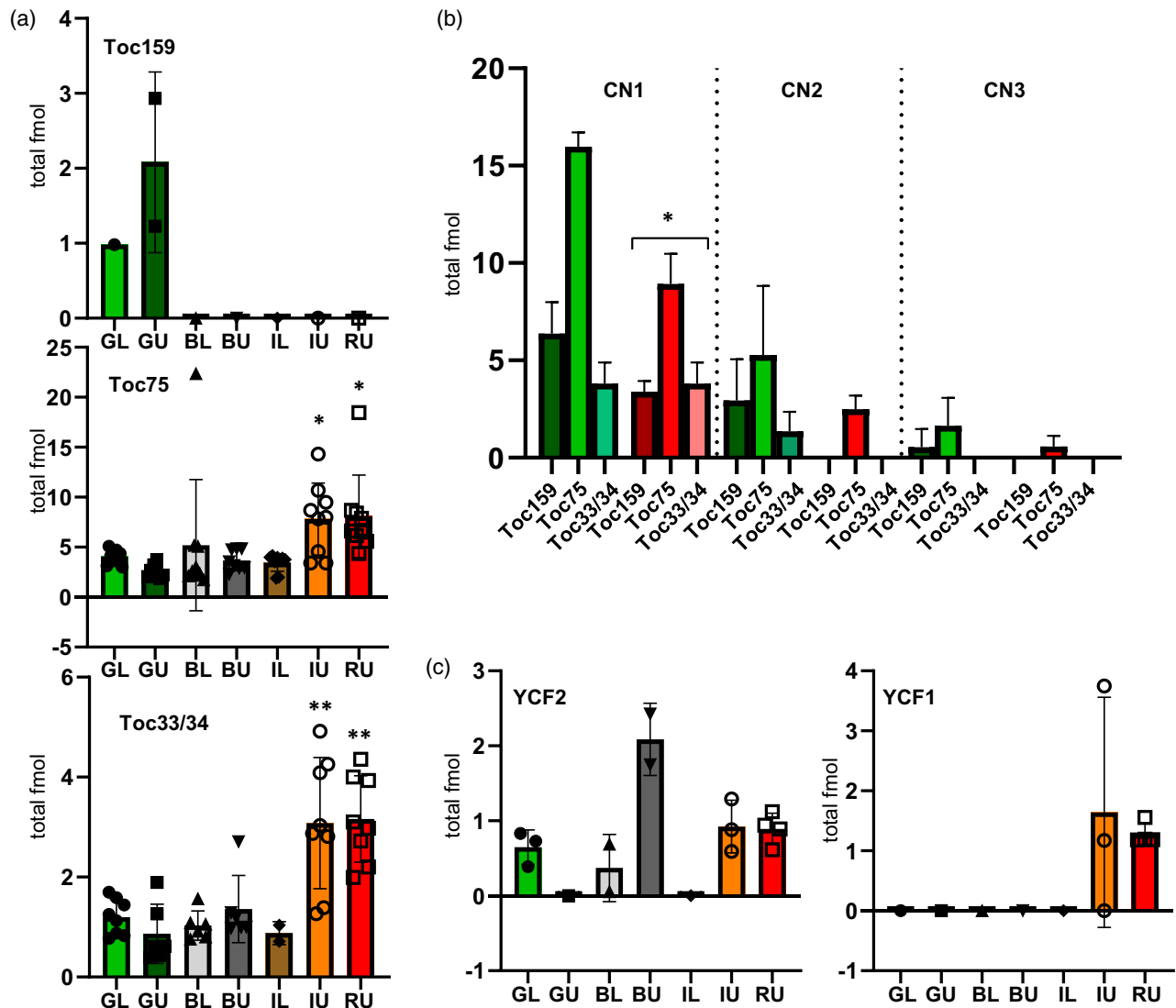


Figure 6. Abundance of subunits of the translocons at the outer (TOC) and inner (TIC) envelope membranes of chloroplasts. Shown are the abundance of the bell pepper homologs for Arabidopsis Toc159 (A0A2G2ZW43), Toc75 (A0A2G2ZE8), and Toc33/34 (A0A1U8G0U4) as identified in in solution digestions (a) and from the CN-PAGE analyses (b). CN PAGE gel slices 1–3 (CN1–3) (see also Figure 2). (c) The abundance of the TIC components YCF1 (A0A2G2YAF6) and YCF2 (A0A2G2YSI8, A0A2G2Z199, A0A2G2ZTJ0, and A0A2G3AIN8) as determined from in solution digestions. In all instances, error bars indicate standard deviation (SD). Significant differences with the GL sample (as chloroplast reference) are highlighted by one (P -value < 0.05 , t -test [Welch test], two-sided) or two stars (P -value < 0.005 , t -test [Welch test], two-sided) or three stars (P -value < 0.0005 , t -test [Welch test], two-sided) on top of the columns.

to tomato high amounts of plastocyanin as electron acceptor for the latter (Figure 4, Figure S5(c)). Intriguingly, we did not find an increase in PTOX levels supporting elevated electron flux through the cytochrome b_6/f complex and plastocyanin in bell pepper compared to tomato chloroplasts (Figure 4). On the other hand, PTOX has different functions in photosynthetic chloroplasts and non-photosynthetic chloroplasts and it is possible that its abundance is maintained during plastid-type transition at a level sufficient for PDS electron scavenging. In order to identify mechanisms that distinguish climacteric from non-climacteric fruit ripening processes, plastid datasets must be supplemented and aligned with data on mitochondrial

metabolism in the same context. All mass spectrometry data files from the present study are made available for download via PRIDE (<https://www.ebi.ac.uk/pride/archive/>), facilitating their re-analysis with different tools for database matching. In summary, our data provide insights into the chloroplast differentiation process at unprecedented depth and spark hypotheses that await further testing.

EXPERIMENTAL PROCEDURES

Material

LC-MS grade solvents, including water with 0.01% (w/v) formic acid, water with 0.1% (w/v) trifluoroacetic acid, and acetonitrile

with 0.1% (w/v) formic acid, were obtained from Carl Roth (Karlsruhe, Germany). Porcine sequencing grade modified trypsin was obtained from Promega (Mannheim, Germany).

Plant material

Capsicum annuum fruits were used for the preparation of chloroplast, chromoplast, and pigment extracts. The plants (cultivar *Selma Bell*) were grown on soil in a greenhouse (20.8–15.7°C, 16 h light, relative humidity: day 65%, night 45%). Fruits of different degrees of maturity (Figure 1(a)) were harvested immediately after the end of the dark period. Chopped plant material (180–200 g) was homogenized in 360–400 ml homogenization buffer (330 mM sorbitol, 2 mM EDTA, 50 mM HEPES [pH 7.5], 1 mM MnCl₂, 1 mM MgCl₂, 2 mM DTT, 0.1% [w/v] BSA, and 0.1% [w/v] Na ascorbate) and filtered through a Miracloth filter (22–25 µm). After centrifugation at 2000 ×g and 4°C for 10 min, the pellet was resuspended in 5 ml homogenization buffer and used for Percoll density gradient centrifugation (2.5 ml each, 40 min, 2600 ×g, 4°C, acceleration at level 3, brakes off). Upper (40/20%) and lower (60/40%) layers containing plastids were transferred into 25 ml HEPES (50 mM, pH 7.5)/sorbitol (330 mM) buffer and centrifuged (5 min, 2000 ×g, 4°C). The plastid pellet was washed once by adding 10 ml HEPES/sorbitol buffer. Plastid pellets were resuspended in HEPES/sorbitol buffer. Aliquots of 250/500 µg protein (as determined using the Bradford method) were frozen in liquid N₂ and stored at –80°C.

Pigment analysis

Pigments of all different maturation stages (green, black, intermediate, red) were extracted using 500 µl MeOH:chloroform (2.5:2 [v/v]), 0.1% butylated hydroxytoluene per 250 µg plastid pellet. After incubation for 10 min on ice in the dark, 250 µl Tris-HCl (pH 7.5, 1 M NaCl) was added. After another 10 min on ice in the dark, samples were centrifuged (10 min, 1350 ×g, 4°C). The aqueous phase was re-extracted twice using 500 µl 0.1% BHT in chloroform and merged organic phases were dried in vacuum and stored until further analysis. UV/VIS absorption spectra were recorded between 220 and 800 nm and the samples were stored at –20°C. In order to quantify changes during maturation, all samples were analyzed on a LaChrom HPLC (Merck-Hitachi: L-7100 pump, D-7000 interface, L-7455 DAD detector) equipped with a ProntoSIL C₁₈ AQ (120 Å, 5 µm). Pigment samples (20 µl re-solubilized in 150 µl acetone) were injected and separated in a linear gradient of 30–90% B (buffer A: methanol:H₂O, 75:25 [v/v]; buffer B: ethyl acetate) within 50 min. The eluent was detected for 70 min in the range of 230–750 nm. Pigments were identified by atmospheric pressure chemical ionization mass spectrometry on an LCO Classic Finnigan MAT (fullscan, positive mode, 50–2000 m/z, 400°C APCI, 7 µA corona voltage, 250°C capillary temperature) coupled to an Agilent 1220 Infinity LC, equipped with the abovementioned RP18 column in a linear gradient of 30–80% B in 30 min and 80–90% B for an additional 20 min (buffer A: methanol:H₂O, 75:25 [v/v]; buffer B: 2-propanol).

Colorless native PAGE

Aliquots of 250 µg protein were resuspended in 125 µl CN buffer (50 mM Bis-Tris [pH 7], 0.5 M ε-aminocaproic acid, 10% glycerol, 5 mM DTT, 2 mM CaCl₂, 20 µl/ml protease inhibitor mix [Serva, SERVA Electrophoresis GmbH, Heidelberg, Germany], 1.5% n-dodecyl β-D-maltoside) to obtain a final concentration of 2 µg/µl protein or 0.5 µg/µl chlorophyll. After incubation (30 min, 4°C, 15 rpm) and centrifugation (30 min, 100 000 ×g, 4°C), 31.2 µl 5× CN buffer (50 mM Bis-Tris [pH 7], 0.5 M ε-aminocaproic acid, 50% glycerol, 0.04% Ponceau S) was added to the supernatants.

The dissolved samples were centrifuged (5 min, 20 000 ×g, 4°C) and applied to gradient gels (5–13.5%). CN polyacrylamide gels were stained with Coomassie Brilliant Blue.

Protein digestion

Every CN polyacrylamide gel lane was cut into 16 equally sized slices, which were subsequently digested with trypsin as previously described (Rödiger *et al.*, 2014). For the in solution digestion, aliquots of 250 µg protein were resuspended in 100 µl 25 mM ammonium bicarbonate (final protein concentration, 5 µg/µl). Next, 20 µl (100 µg protein) was solubilized (10 min, 80°C) in 201 µl 25 mM ammonium bicarbonate containing 0.05% (w/v) RapiGest SF (Waters, Milford, MA, USA) and reduced by adding 6.2 µl 10 mM dithiothreitol and incubating for 10 min at 60°C. Cysteine residues were alkylated using 6.2 µl of 30 mM iodoacetamide for 30 min in the dark. Subsequently, 2 µl trypsin (final concentration, 1:100 [w/w] corresponding to 1 µg protease per vial) was added. Samples with a final volume of 250 µl were digested at 37°C overnight. To stop the digestion, 2 µl of 37% HCl was added to reach a pH value < 2. To avoid loading insoluble material onto the column, the peptide solutions were thoroughly centrifuged prior to sample loading (4°C, 21 500 ×g, 30 min).

Nano-LC separation, HD-MS^E data acquisition, and protein identification/quantification

Nano-LC HD-MS^E data were acquired for three biological replicates, and for every biological replicate three technical replicates were performed. Data acquisition was performed as described previously (Helm *et al.*, 2014) using a nanoACQUITY UPLC (trap column: 200 mm × 180 µm fused silica, 5 µm Symmetry C₁₈; separation column: 250 mm × 75 µm fused silica, 1.8 µm HSS T3 C₁₈)/Synapt G2-S mass spectrometer (Waters). Data analysis was carried out using the ProteinLynx Global Server (PLGS 3.0.1, Apex3D algorithm v. 2.128.5.0, 64 bit, Waters) with auto-determination of chromatographic peak width and MS TOF resolution. Lock mass window was set to 0.25 Da. Low/high energy thresholds were set to 180/15 counts, respectively. Elution start time was 5 min, and the intensity threshold was set to 750 counts. Databank search query (PLGS workflow) was carried out as follows: Peptide and fragment tolerances were set to automatic, and at least two fragment ion matches per peptide and five fragment ion matches from at least two peptides were required for protein identification. Maximum protein mass was set to 250 kDa. Primary digest reagent was trypsin (one missed cleavage). According to the digestion protocol fixed (carbamidomethyl on Cys) as well as variable (oxidation on Met) modifications were set. We defined 10 fmol/injection rabbit glycogen phosphorylase B (P00489) as internal quantification standard. The database for bell pepper (*C. annuum*) was downloaded from <https://www.uniprot.org/proteomes/UP000222542>, containing 35 548 protein entries (Qin *et al.*, 2014). The false discovery rate (FDR) was 4% at the protein level. In cases where no proteotypic peptides were identified to distinguish protein isoforms, these are subsumed under a single identifier and thus can be considered protein groups. The mass spectrometry proteomics data have been deposited to the ProteomeXchange Consortium (Vizcaino *et al.*, 2016) via the PRIDE partner repository (<https://www.ebi.ac.uk/pride/archive/>) under the dataset identifiers PXD006409 and PXD006477.

Hierarchical clustering

Clustering analyses were performed using the Multiple Experiment Viewer (<http://mev.tm4.org/>). For the hierarchical clustering, we loaded the average abundance values for every protein in the

different plastid preparations into the data file, and performed clustering with a Pearson correlation metric using average linkage clustering.

ACKNOWLEDGMENTS

S.B. gratefully acknowledges DFG support for the acquisition of a Synapt G2-S mass spectrometer (INST 271/283-1 FUGG) and for support through DFG grant BA 1902/3-2. We furthermore sincerely thank Christian E.H. Schmelzer (Fraunhofer Institute for Microstructure of Materials and Systems [IMWS] Halle [Saale]) for the excellent cooperation in the analysis of pigments with mass spectrometry. The authors furthermore thank Arne Preuß for help with bell pepper growth. Open Access funding enabled and organized by ProjektDEAL.

AUTHOR CONTRIBUTIONS

AR, BA, FM, and SB designed the research; AR, BA, DD, SH, FM, NP, and SB performed the research and analyzed the data; AR and SB wrote the paper.

CONFLICT OF INTEREST

The authors declare that there is no conflict of interest associated with the manuscript.

DATA AVAILABILITY STATEMENT

All MS data were uploaded to PRIDE (<https://www.ebi.ac.uk/pride/archive/>) and are accessible with the dataset identifiers PXD006409 and PXD006477.

SUPPORTING INFORMATION

Additional Supporting Information may be found in the online version of this article.

Figure S1. Chromatograms of pigment extracts of chloroplasts (green) and chromoplasts (red).

Figure S2. Profile of protein abundances along the CN-PAGE gel in every gel slice.

Figure S3. Localization prediction for proteins identified from the different plastid preparations.

Figure S4. Alignment of putative transit peptides of chloroplast and chromoplast proteins.

Figure S5. Selected protein abundances during tomato chromoplast differentiation.

Table S1. Identification of pigment peaks by LC-APCI mass spectrometry.

Table S2. CN-PAGE gel slices analyzed by MS^E.

Table S3. Protein identification, abundance determination, and localization prediction.

Table S4. Protein quantification from CN-PAGE gel slices 1–3.

REFERENCES

Agne, B. and Kessler, F. (2009) Protein transport in organelles: the Toc complex way of preprotein import. *FEBS J.* **276**, 1156–1165.

Almagro Armenteros, J.J., Salvatore, M., Emanuelsson, O., Winther, O., von Heijne, G., Elofsson, A. and Nielsen, H. (2019) Detecting sequence signals in targeting peptides using deep learning. *Life Sci. Alliance*, **2**, e201900429.

Baginsky, S., Siddique, A. and Gruijsem, W. (2004) Proteome analysis of tobacco bright yellow-2 (BY-2) cell culture plastids as a model for undifferentiated heterotrophic plastids. *J. Proteome Res.* **3**, 1128–1137.

Barsan, C., Sanchez-Bel, P., Rombaldi, C., Egea, I., Rossignol, M., Kuntz, M., Zouine, M., Latché, A., Bouzayen, M. and Pech, J.C. (2010) Characteristics of the tomato chromoplast revealed by proteomic analysis. *J. Exp. Bot.* **61**, 2413–2431.

Barsan, C., Zouine, M., Maza, E. *et al.* (2012) Proteomic analysis of chloroplast-to-chromoplast transition in tomato reveals metabolic shifts coupled with disrupted thylakoid biogenesis machinery and elevated energy-production components. *Plant Physiol.* **160**, 708–725.

Bischof, S., Baerenfaller, K., Wildhaber, T. *et al.* (2011) Plastid proteome assembly without Toc159: photosynthetic protein import and accumulation of N-acetylated plastid precursor proteins. *Plant Cell*, **23**, 3911–3928.

Camara, B., Hugueney, P., Bouvier, F., Kuntz, M. and Moneger, R. (1995) Biochemistry and molecular biology of chromoplast development. *Int. Rev. Cytol.* **163**, 175–247.

D'Andrea, L. and Rodriguez-Concepcion, M. (2019) Manipulation of Plastidial Protein Quality Control Components as a New Strategy to Improve Carotenoid Contents in Tomato Fruit. *Front. Plant Sci.* **10**, 1071.

Dutta, S., Teresinski, H.J. and Smith, M.D. (2014) A split-ubiquitin yeast two-hybrid screen to examine the substrate specificity of atToc159 and atToc132, two Arabidopsis chloroplast preprotein import receptors. *PLoS One*, **9**, e95026.

Egea, I., Barsan, C., Bian, W., Purgatto, E., Latche, A., Chervin, C., Bouzayen, M. and Pech, J.C. (2010) Chromoplast differentiation: current status and perspectives. *Plant Cell Physiol.* **51**, 1601–1611.

Green, L.S., Yee, B.C., Buchanan, B.B., Kamide, K., Sanada, Y. and Wada, K. (1991) Ferredoxin and ferredoxin-NADP reductase from photosynthetic and non-photosynthetic tissues of tomato. *Plant Physiol.* **96**, 1207–1213.

Grimmer, J., Helm, S., Dobritzsch, D., Hause, G., Shema, G., Zahedi, R.P. and Baginsky, S. (2020) Mild proteasomal stress improves photosynthetic performance in Arabidopsis chloroplasts. *Nat. Commun.* **11**, 1662.

Helm, S., Dobritzsch, D., Rödiger, A., Agne, B. and Baginsky, S. (2014) Protein identification and quantification by data-independent acquisition and multi-parallel collision-induced dissociation mass spectrometry (MSE) in the chloroplast stroma proteome. *J. Proteomics*, **98**, 79–89.

Josse, E.M., Simkin, A.J., Gaffé, J., Labouré, A.M., Kuntz, M. and Carol, P. (2000) A plastid terminal oxidase associated with carotenoid desaturation during chromoplast differentiation. *Plant Physiol.* **123**, 1427–1436.

Kahlau, S. and Bock, R. (2008) Plastid transcriptomics and translomics of tomato fruit development and chloroplast-to-chromoplast differentiation: chromoplast gene expression largely serves the production of a single protein. *Plant Cell*, **20**, 856–874.

Kikuchi, S., Bedard, J., Hirano, M. *et al.* (2013) Uncovering the protein translocator at the chloroplast inner envelope membrane. *Science*, **339**, 571–574.

Kikuchi, S., Asakura, Y., Imai, M. *et al.* (2018) A Ycf2-FtsHi Heteromeric AAA-ATPase Complex Is Required for Chloroplast Protein Import. *Plant Cell*, **30**, 2677–2703.

Kleffmann, T., von Zychlinski, A., Russenberger, D., Hirsch-Hoffmann, M., Gehrig, P., Gruijsem, W. and Baginsky, S. (2007) Proteome dynamics during plastid differentiation in rice. *Plant Physiol.*, **143**, 912–923.

Kuai, B., Chen, J. and Hörtensteiner, S. (2018) The biochemistry and molecular biology of chlorophyll breakdown. *J. Exp. Bot.* **69**, 751–767.

Li, L. and Yuan, H. (2013) Chromoplast biogenesis and carotenoid accumulation. *Arch. Biochem. Biophys.* **539**, 102–109.

Ling, Q., Huang, W., Baldwin, A. and Jarvis, P. (2012) Chloroplast biogenesis is regulated by direct action of the ubiquitin-proteasome system. *Science*, **338**, 655–659.

Ma, D., Huang, X., Hou, J. *et al.* (2018) Quantitative analysis of the grain amyloplast proteome reveals differences in metabolism between two wheat cultivars at two stages of grain development. *BMC Genom.* **19**, 768.

Nawrocki, W.J., Tourasse, N.J., Taly, A., Rappaport, F. and Wollman, F.A. (2015) The plastid terminal oxidase: its elusive function points to multiple contributions to plastid physiology. *Annu. Rev. Plant Biol.* **66**, 49–74.

Neuhaus, H.E. and Emes, M.J. (2000) Nonphotosynthetic metabolism in plastids. *Annu. Rev. Plant Physiol. Plant Mol. Biol.* **51**, 111–140.

Nievelstein, V., Vandekerckhove, J., Tadros, M.H., Lintig, J.V., Nitschke, W. and Beyer, P. (1995) Carotene desaturation is linked to a respiratory redox pathway in *Narcissus pseudonarcissus* chromoplast membranes. Involvement of a 23-kDa oxygen-evolving-complex-like protein. *Eur. J. Biochem.* **233**, 864–872.

- Norris, S.R., Barrette, T.R. and DellaPenna, D. (1995) Genetic dissection of carotenoid synthesis in Arabidopsis defines plastoquinone as an essential component of phytoene desaturation. *Plant Cell*, **7**, 2139–2149.
- Osoerio, S., Alba, R., Nikoloski, Z., Kochevenco, A., Fernie, A.R. and Giovannoni, J.J. (2012) Integrative comparative analyses of transcript and metabolite profiles from pepper and tomato ripening and development stages uncovers species-specific patterns of network regulatory behavior. *Plant Physiol.* **159**, 1713–1729.
- Pateraki, I., Renato, M., Azcón-Bieto, J. and Boronat, A. (2013) An ATP synthase harboring an atypical γ -subunit is involved in ATP synthesis in tomato fruit chromoplasts. *Plant J.* **74**, 74–85.
- Pesaresi, P., Mizzotti, C., Colombo, M. and Masiero, S. (2014) Genetic regulation and structural changes during tomato fruit development and ripening. *Front Plant Sci.* **5**, 1–14.
- Qin, C., Yu, C., Shen, Y. et al. (2014) Whole-genome sequencing of cultivated and wild peppers provides insights into *Capsicum* domestication and specialization. *Proc. Natl. Acad. Sci. USA*, **111**, 5135–5140.
- Quinet, M., Angosto, T., Yuste-Lisbona, F.J., Blanchard-Gros, R., Bigot, S., Martinez, J.P. and Lutts, S. (2019) Tomato fruit development and metabolism. *Front. Plant Sci.* **10**, 1554.
- Renato, M., Pateraki, I., Boronat, A. and Azcon-Bieto, J. (2014) Tomato fruit chromoplasts behave as respiratory bioenergetic organelles during ripening. *Plant Physiol.* **166**, 920–933.
- Renato, M., Boronat, A. and Azcón-Bieto, J. (2015) Respiratory processes in non-photosynthetic plastids. *Front. Plant Sci.* **6**, 496.
- Rödiger, A., Agne, B., Baerenfaller, K. and Baginsky, S. (2014) Arabidopsis proteomics: a simple and standardizable workflow for quantitative proteome characterization. *Methods Mol. Biol.* **1072**, 275–288.
- Rodríguez-Concepcion, M. et al. (2018) A global perspective on carotenoids: Metabolism, biotechnology, and benefits for nutrition and health. *Prog. Lipid Res.* **70**, 62–93.
- Rodríguez-Concepcion, M., D'Andrea, L. and Pulido, P. (2019) Control of plastidial metabolism by the Clp protease complex. *J. Exp. Bot.* **70**, 2049–2058.
- Sadali, N.M., Sowden, R.G., Ling, Q. and Jarvis, R.P. (2019) Differentiation of chromoplasts and other plastids in plants. *Plant Cell Rep.* **38**, 803–818.
- Schäfer, P., Helm, S., Köhler, D., Agne, B. and Baginsky, S. (2019) Consequences of impaired 1-MDa TIC complex assembly for the abundance and composition of chloroplast high-molecular mass protein complexes. *PLoS One*, **14**, e0213364.
- Shanmugabalaji, V., Chahtane, H., Accossato, S., Rahire, M., Gouzerh, G., Lopez-Molina, L. and Kessler, F. (2018) Chloroplast biogenesis controlled by DELLA-TOC159 interaction in early plant development. *Curr. Biol.* **28**, 2616–2623.
- Shahbazi, M., Gilbert, M., Labouré, A.M. and Kuntz, M. (2007) Dual role of the plastid terminal oxidase in tomato. *Plant Physiol.* **145**, 691–702.
- Silva, J.C. et al. (2006) Absolute quantification of proteins by LCMSE – a virtue of parallel MS acquisition. *Mol. Cell Proteomics*, **5**, 144–156.
- Siddique, M.A., Grossmann, J., Gruissem, W. and Baginsky, S. (2006) Proteome analysis of bell pepper (*Capsicum annuum* L.) chromoplasts. *Plant Cell Physiol.* **47**, 1663–1673.
- Sun, T., Zhou, F., Huang, X.Q., Chen, W.C., Kong, M.J., Zhou, C.F., Zhuang, Z., Li, L. and Lu, S. (2019) ORANGE represses chloroplast biogenesis in etiolated Arabidopsis cotyledons via interaction with TCP14. *Plant Cell*, **31**, 2996–3014.
- Suzuki, M., Takahashi, S., Kondo, T., Dohra, H., Ito, Y., Kiriwa, Y., Hayashi, M., Kamiya, S., Kato, M. and Fujiwara, M. (2015) Plastid proteomic analysis in tomato fruit development. *PLoS One*, **10**, 1–25.
- Szymanski, J., Levin, Y., Savidor, A., Breitel, D., Chappell-Maor, L., Heinig, U., Töpfer, N. and Aharoni, A. (2017) Label-free deep shotgun proteomics reveals protein dynamics during tomato fruit tissues development. *Plant J.* **90**, 396–417.
- Taylor, M. and Ramsay, G. (2005) Carotenoid biosynthesis in plant storage organs: recent advances and prospects for improving plant food quality. *Physiol. Plant*, **124**, 143–151.
- Thimm, O., Blaesing, O., Gibon, Y., Nagel, A., Meyer, S., Krüger, P., Selbig, J., Müller, L.A., Rhee, S.Y. and Stitt, M. (2004) MAPMAN: a user-driven tool to display genomics data sets onto diagrams of metabolic pathways and other biological processes. *Plant J.* **37**, 914–939.
- van Wijk, K.J. and Kessler, F. (2017) Plastoglobuli: plastid microcompartments with integrated functions in metabolism, plastid developmental transitions, and environmental adaptation. *Annu. Rev. Plant Biol.* **68**, 253–289.
- Vizcaino, J.A., Csordas, A. del-Toro, N. et al. (2016) Update of the PRIDE database and its related tools. *Nucleic Acids Res.* **44**, D447–D456.
- von Zychlinski, A., Kleffmann, T., Krishnamurthy, N., Sjölander, K., Baginsky, S. and Gruissem, W. (2005) Proteome analysis of the rice etioplast: metabolic and regulatory networks and novel protein functions. *Mol. Cell Proteomics*, **4**, 1072–1084.
- Wang, Y.Q., Yang, Y., Fei, Z., Yuan, H., Fish, T., Thannhauser, T.W., Mazourek, M., Kochian, L.V., Wang, X. and Li, L. (2013) Proteomic analysis of chromoplasts from six crop species reveals insights into chromoplast function and development. *J. Exp. Bot.* **64**, 949–961.
- Waters, M. and Pyke, K. (2005) *Plastid development and differentiation*. Blackwell: Oxford.